




Article

The Influence of Internal Stress on the Nanocrystal Formation of Amorphous $\text{Fe}_{73.8}\text{Si}_{13}\text{B}_{9.1}\text{Cu}_1\text{Nb}_{3.1}$ Microwires and Ribbons

Artem Fuks^{1,2,*} , Galina Abrosimova¹ , Oleg Aksenov¹ , Margarita Churyukanova³ and Alexandr Aronin^{1,2}¹ Osipyan Institute of Solid State Physics RAS, 142432 Chernogolovka, Russia² Faculty of Physics, National Research University Higher School of Economics, 109028 Moscow, Russia³ Department of Physical Chemistry, National University of Science and Technology MISIS, 119049 Moscow, Russia

* Correspondence: artemfux@yandex.ru

Abstract: The early stages of nanocrystallization in amorphous $\text{Fe}_{73.8}\text{Si}_{13}\text{B}_{9.1}\text{Cu}_1\text{Nb}_{3.1}$ ribbons and microwires were compared in terms of their internal stress effects. The microstructure was investigated by the X-ray diffraction method. Classical expressions of crystal nucleation and growth were modified for microwires while accounting for the internal stress distribution, in order to justify the XRD data. It was assumed that, due to the strong compressive stresses on the surface part and tensile stresses on the central part, crystallization on the surface part of the microwire proceeded faster than in the central part. The results revealed more rapid nanocrystallization in microwires compared to that in ribbons. During the initial period of annealing, the compressive surface stress of a microwire caused the formation of a predominantly crystallized surface layer. The results obtained open up new possibilities for varying the high-frequency properties of microwires and their application in modern sensorics.

Keywords: amorphous microwires; X-ray diffraction; stress distribution; nanocrystallization



Citation: Fuks, A.; Abrosimova, G.; Aksenov, O.; Churyukanova, M.; Aronin, A. The Influence of Internal Stress on the Nanocrystal Formation of Amorphous $\text{Fe}_{73.8}\text{Si}_{13}\text{B}_{9.1}\text{Cu}_1\text{Nb}_{3.1}$ Microwires and Ribbons. *Crystals* **2022**, *12*, 1494. <https://doi.org/10.3390/cryst12101494>

Academic Editor: Cyril Cayron

Received: 28 September 2022

Accepted: 19 October 2022

Published: 21 October 2022

Publisher's Note: MDPI stays neutral with regard to jurisdictional claims in published maps and institutional affiliations.



Copyright: © 2022 by the authors. Licensee MDPI, Basel, Switzerland. This article is an open access article distributed under the terms and conditions of the Creative Commons Attribution (CC BY) license (<https://creativecommons.org/licenses/by/4.0/>).

1. Introduction

An amorphous-nanocrystalline $\text{Fe}_{73.5}\text{Si}_{13.5}\text{B}_9\text{Cu}_1\text{Nb}_3$ alloy was first mentioned in [1]. It was established as a soft magnetic material that demonstrated high values of magnetic permeability and saturation magnetization, combined with low magnetostriction and low magnetization losses [2,3]. An amorphous alloy of this composition can be produced in the form of a ribbon by the melt spinning method, and in the form of a microwire by the Ulitovsky-Taylor method. An amorphous-nanocrystalline state is reached as a result of heat treatment. Due to the peculiarities of the production processes, microwires and ribbons have different stress states, although their chemical compositions can be identical [4,5]. The value of quenching stresses in a ribbon is in the tens of MPa. The stress level in microwires is 1–2 orders of magnitude higher than that in ribbons. In microwires, stresses are distributed in homogeneously over the radius. Strong compressive (in units of GPa) stresses prevail in the near-surface region of a microwire, while tensile stresses (in hundreds of MPa) prevail in the central part [5,6]. When the shell is removed, the total level of stresses decreases by several hundreds of MPa [6]. Despite shell removing, the character of the total stress distribution does not change (strong compressive stress on the surface part and weak tensile stress in the central part). This difference in the stress state not only affects the magnetization reversal process and the shape of a hysteresis loop [7,8] but it should also affect the processes of crystal formation at the initial stages. Previously, the effect of mechanical stresses on the crystallization and magnetic properties of Co-rich microwires was observed in [9–11]. It was found that isothermal annealing led to the formation of crystallites with an elongated shape, and there existed a preferential orientation along the microwire axis [12]. This tendency was stronger in microwires that had undergone a directional crystallization in the presence of a magnetic field [13]. It was shown that the

growth of crystals oriented along the microwire axis led to a giant increase in the coercivity (by an order of magnitude or more). Moreover, the cumulative effects of stresses on the crystallization and high-frequency properties of microwires was demonstrated in [11].

The crystallization of the $\text{Fe}_{73.5}\text{Si}_{13.5}\text{B}_9\text{Cu}_1\text{Nb}_3$ alloy considered in this work led to the formation of nanocrystals with the density being higher than that of the amorphous matrix. Thus, the density of the amorphous $\text{Fe}_{73.5}\text{Si}_{13.5}\text{B}_9\text{Cu}_1\text{Nb}_3$ alloy was $7.14 \cdot 10^3 \text{ kg/m}^3$ [14], the density of the Fe_3Si nanocrystals was $7.39 \cdot 10^3 \text{ kg/m}^3$ [15]. Therefore, under crystallization, a negative bulk effect would be the reason for the facilitated formation of nanocrystals. Then, the combination of existing internal stresses and additional stresses arising due to the compensation of a bulk crystallization effect would affect the kinetics of crystal formation under the crystallization of amorphous alloys.

It is well-known that mechanical stresses arising under rolling [16], bending [17], milling [18], plastic deformation [19,20], and static load [21,22] affect crystal formation.

Upon undergoing a negative bulk effect, the Gibbs energy of formation of a critical nucleus of Fe(Si) nanocrystals decreases with an increase in the compressive stresses and, on the contrary, increases under tension. Surely, this affects nucleation frequency and, hence, the size of nanocrystals and their volume fraction in the material. Strong compressive stresses prevail in the near-surface region of a microwire. At that region, as mentioned above, a negative bulk effect was observed under the crystallization of the $\text{Fe}_{73.8}\text{Si}_{13}\text{B}_{9.1}\text{Cu}_1\text{Nb}_{3.1}$ alloy. Then, nanocrystal formation should have been facilitated in the near-surface region of a microwire. At the same time, there were no regions with compressive stresses in the amorphous ribbons [4]. Therefore, when comparing the initial crystallization stages of the amorphous ribbons and microwires, the effect of compressive stresses on them could be estimated. Thus, the present work aimed to study the effect of a high level of mechanical stresses on nanocrystal formation in the amorphous $\text{Fe}_{73.8}\text{Si}_{13}\text{B}_{9.1}\text{Cu}_1\text{Nb}_{3.1}$ alloy, and compared initial nanocrystallization stages in amorphous microwires and ribbons, which had the same composition but significantly different levels of internal stresses.

2. Materials and Methods

Amorphous $\text{Fe}_{73.8}\text{Si}_{13}\text{B}_{9.1}\text{Cu}_1\text{Nb}_{3.1}$ alloys were produced in the form of a ribbon by rapid melt quenching; their thickness was 16–18 μm , and the width was 9 mm. Amorphous alloys of the same composition were produced in the form of a glass-coated microwire by the Ulitovsky-Taylor method; the average diameter of the metallic part was 16.5 μm , and the thickness of the shell was 3.5 μm . Initial samples were produced using high-purity (99.9%) components. As shown in [3], the best values of coercivity and magnetic permeability are achieved by heat treatment of the $\text{Fe}_{73.5}\text{Si}_{13.5}\text{B}_9\text{Cu}_1\text{Nb}_3$ alloy in the temperature range of 773–833 K. DTA analysis performed in [23] revealed that crystallization began at 803 K. In contrast, results from paper [24] indicated that isothermal annealing for 1 h at 723–823 K led to Fe(Si) nanocrystal precipitation. Accordingly, the ribbons and uncoated microwires were annealed in a vacuum at temperatures in the range of 753–823 K for 1 h. The most illustrative results were obtained after annealing at 753 K. Before annealing, the glass shell was removed by chemical etching in hydrofluoric acid.

Since crystals are formed at an enhanced temperature, the value of the stresses corresponding to these conditions needed to be estimated. To study the effect of temperature on the level of mechanical stresses, the degree of bending stress relaxation in the ribbons was estimated. For this to be done, samples of the ribbons were placed into a quartz ampoule along its inner diameter. The length of the samples coincided with the circumference of the ampoule. After that, heat treatment was performed at 753 K. Then, the samples were pulled out of the ampoule, and the curvature radii of the annealed samples were measured. To estimate the degree of stress relaxation, the parameter $\gamma = 1 - R_0/R$ was used [25], where R_0 is the radius of a quartz ampoule and R is the curvature radius of a ribbon after heat treatment.

The structure and phase compositions of the samples before and after annealing were investigated with a SIEMENS D-500 (Manufacturer: Siemens AG. Location: Östliche Rheinbrückenstraße 50, 76187 Karlsruhe) diffractometer using Co K_{α} -radiation. Since the samples contained the amorphous and crystalline phases, the experimental curves were decomposed into a diffuse component caused by scattering from the amorphous phase, and a diffraction component caused by the presence of crystals. When decomposing, the characteristics of the curve of scattering by the initial amorphous phase (the half-width and the position of the diffuse maximum) were taken into account. The size of the nanocrystals was calculated according to the half-width of a diffraction spectrum component using the Scherrer equation [26,27].

The fraction of the amorphous and crystalline phases was estimated by the ratio of the integral intensities of the diffraction and diffuse components of the X-ray diffraction patterns, according to [28].

3. Results

After the production, the samples were amorphous. The X-ray diffraction patterns of initial samples contained only broad diffuse maxima; no diffraction reflections from the crystalline phases were observed (Figure 1).

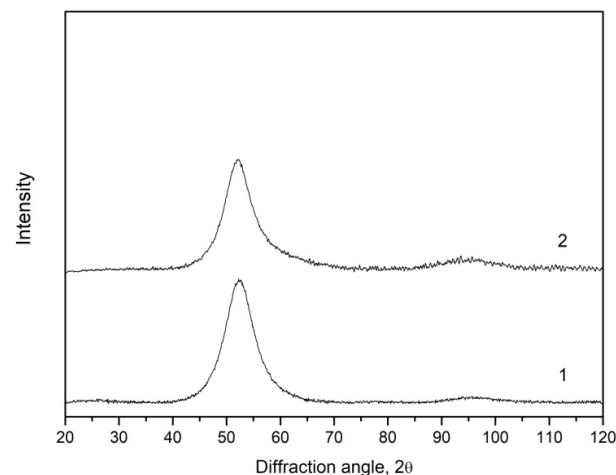


Figure 1. X-ray diffraction patterns of the initial amorphous $Fe_{73.8}Si_{13}B_{9.1}Cu_1Nb_{3.1}$ ribbons (1) and microwires (2).

After the annealing, the structure of both samples changed markedly. Figure 2 shows the X-ray diffraction patterns of the microwires (Figure 2a) and ribbons (Figure 2b) annealed at 753 K for 1 h.

Figure 2 illustrates regions of the main diffuse maximum in the X-ray diffraction patterns; the insets show complete curves. In the figure, curve 1 is an experimental X-ray diffraction pattern, curve 3 corresponds to scattering by the amorphous phase, curve 4 describes diffraction reflections from nanocrystals, and curve 2 is the sum of curves 3 and 4. In the complete X-ray diffraction pattern of the microwires (Figure 2a), diffraction reflections were indexed. They corresponded to the bcc phase with the parameter $a = 2.845 \text{ \AA}$ and a Fe(Si) solid solution. One can see that the intensity of the diffraction reflections (curve 4) in Figure 2a was significantly higher than that of the diffraction reflections in Figure 2b. The analysis of the reflection intensities showed that the fraction of the precipitated nanocrystalline phase in the microwires was 20% higher than that in the ribbons. The half-widths of the diffraction reflections in Figure 2a,b were also different, which was the evidence of different sizes of the nanocrystals. The size of the nanocrystals in the microwires was determined using the Scherrer equation as 16 nm, and that in the ribbons was 6 nm.

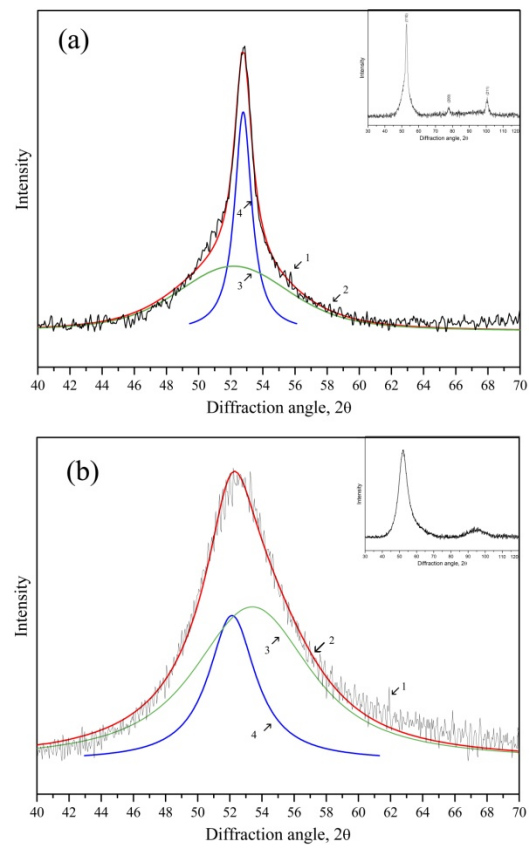


Figure 2. X-ray diffraction patterns of the microwires (a) and ribbons (b) of $\text{Fe}_{73.8}\text{Si}_{13}\text{B}_{9.1}\text{Cu}_1\text{Nb}_{3.1}$ composition annealed at 753 K for 1 h (1—experimental curve, 3—scattering from the amorphous phase, 4—diffraction reflections from nanocrystals, 2—summary of curves 3–4).

To estimate the degree of mechanical stress relaxation under annealing, in the assumption that the initial internal stresses in a microwire decrease with the temperature at the same rate as ribbons induced under bending do, an experiment on the estimation of the degree of bending stress relaxation was performed.

Figure 3 depicts the change in the parameter γ with time. One can see that about 20 min later, bending stresses were almost completely relaxed. To facilitate further calculations, $\gamma = 0.1$ was selected as the “effective” value.

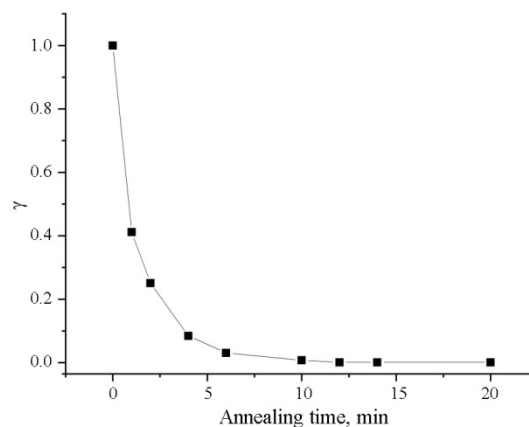


Figure 3. Relaxation curve of bending stresses for initial samples of the ribbon under annealing at 753 K.

4. Discussion

We shall assume that nanocrystals nucleate by a homogeneous mechanism. As is well-known, Cu clusters are formed in this alloy under heating, which can act as heterogeneous nucleation centers [29]. However, under consideration of the first approximation, we will not take into account their effect on the kinetics of the Fe(Si) nanocrystal nucleation.

To consider the effect of the internal stresses of the microwire on nucleation frequency, one should first modify the expression for the Gibbs energy ΔG of a spherical nucleus with the radius r , proposed in [16–22]:

$$\Delta G = -4/3\pi r^3(\Delta G_{ch} + E_\epsilon) + 4\pi r^2\sigma \quad (1)$$

where ΔG_{ch} is the driving force of crystallization from an amorphous state, E_ϵ is the elastic energy that includes deformation contributions from internal stresses and the emergence of a nanocrystal different from the amorphous density matrix, and σ is the surface energy.

We shall write the elastic energy in more detail [30], assuming that the shear component of deformation γ is absent:

$$E_\epsilon = \pi G \epsilon(x)^2 / 4 \quad (2)$$

where $G = E/(2(1 + \nu))$ is the shear modulus, and $E = 139$ GPa is Young's modulus at 753 K. Under normal conditions, the value of Young's modulus is 154 GPa [31]; however, considering the temperature effect, there is a decrease by about 10% [32], ν is the Poisson's ratio that is taken to be 0.3 [33,34], x , is the radial from the microwire axis, and $\epsilon(x)$ is the normal component of deformation. It is presented in the form:

$$\epsilon(x) = \Delta V / 3V + \gamma\sigma(x) / E \quad (3)$$

where $\sigma(x) = \sigma_{rr} + \sigma_{\theta\theta} + \sigma_{zz}$ is the sum of diagonal components of a stress tensor of the metallic core of a microwire with respect to the sign, calculated according to [6,8], γ is the effective value of the stress relaxation parameter, obtained from an experiment with the ribbons. $\Delta V / V$ is the value of a bulk effect calculated from the difference between densities of amorphous material and formed nanocrystals:

$$\Delta V / V = (\rho_{am} - \rho_{cr}) / \rho_{am} \quad (4)$$

where $\rho_{am,cr}$ are the densities of an amorphous alloy and nanocrystals, respectively. According to [14], the density of the amorphous $\text{Fe}_{73.5}\text{Si}_{13.5}\text{B}_9\text{Cu}_1\text{Nb}_3$ alloy was $7.14 \cdot 10^3$ kg/m³, the density of nanocrystals of a solid solution of 25% Si in Fe, Fe_3Si , was $7.39 \cdot 10^3$ kg/m³ [15], and the density of Fe was $7.87 \cdot 10^3$ kg/m³. Considering that density changes linearly with a change in Si concentration, the density of nanocrystals was taken to be $7.55 \cdot 10^3$ kg/m³ at Si content of 16.5% [35].

It is assumed in Equation (3) that compressive stresses are negative, and tension stresses are positive. From (1), we obtain the Gibbs energy of a critical nucleus:

$$\Delta G^* = 16\pi\sigma^3 / (3(\Delta G_{ch} + E_\epsilon)^2) \quad (5)$$

The next assumption is that the value of internal stresses in a ribbon is significantly lower than that in a microwire [4]. Therefore, the second term in (3) could be neglected for calculations in a ribbon. The difference between free energies of the alloy in amorphous and crystalline states was calculated according to [36]:

$$\Delta G_{ch} = 2T\Delta H_{cr}\Delta T\rho_{am} / (T_m(T_m + T)) \quad (6)$$

where $\Delta H_{cr} = 58$ J/g is the crystallization enthalpy [37], T_m is the melting temperature taken to be 1450 K [38], T is the temperature of heat treatment at 753 K, and ρ_{am} is the density of the amorphous matrix at $7.14 \cdot 10^3$ kg/m³. Here, we assumed that the crystallization

enthalpy for ribbons and microwires was the same and did not depend on internal stresses. Then, ΔG_{ch} is 0.14 GJ/m^3 .

The growth rate was calculated by the formula [39,40]:

$$u_c = \frac{fD}{a_0} \left[1 - \exp\left(\frac{-(\Delta G_{ch} + E_\epsilon)}{kT}\right) \right] \quad (7)$$

where $f \approx 1$ and D is the diffusion coefficient. The growth rate for the ribbon was $2.23 \cdot 10^{-11} \text{ m/s}$, assuming that only the bulk effect was presented and $\sigma(x) = 0$ in (3). By using the stress distribution $\sigma(x)$ as a function of the distance to the microwire axis calculated according to [6,8], as well as Equation (2), the distribution $u_c(x)$ was calculated (Figure 4). The obtained values of nanocrystal growth rate were within the range of $2.22 \cdot 10^{-11} - 2.30 \cdot 10^{-11} \text{ m/s}$.

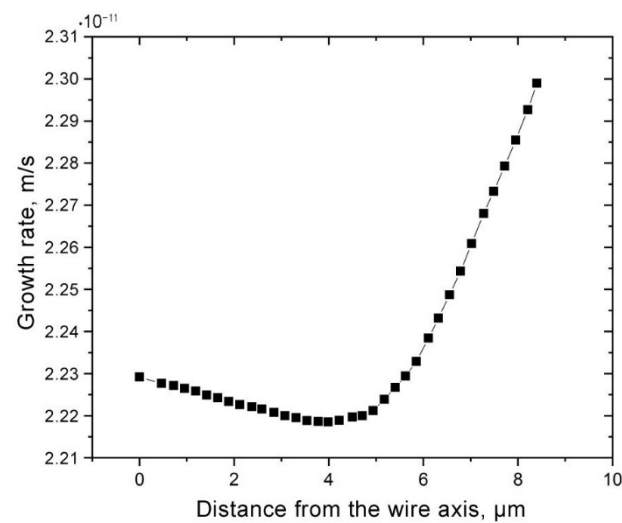


Figure 4. Distribution of nanocrystal growth rate over the microwire radius calculated by the Formula (7).

It follows from the data of the X-ray diffraction studies that the content of nanocrystals in the microwire was 20% higher than that in the ribbon. Assuming that, at the initial crystallization stages, the growth rate and nucleation frequency of the nanocrystals did not change with time, we used the well-known expression for the crystallized volume fraction $X = 1 - \exp(-\frac{\pi}{3} I u_c^3 t^4)$ [41], and wrote a ratio for the crystallized fractions in a microwire and ribbon:

$$\frac{X_{wire}}{X_{ribbon}} = \frac{[1 - \exp(-\frac{\pi}{3} I u_c^3 t^4)]_{wire}}{[1 - \exp(-\frac{\pi}{3} I u_c^3 t^4)]_{ribbon}} \quad (8)$$

The left side of Equation (8) is the relative fraction of nanocrystals determined experimentally, with the average over the volume fraction resulting in the microwire. On the right side, there are unknown values of nanocrystal nucleation frequencies, which, in turn, contain an unknown value of surface energy. The value of σ was determined from the condition that the value on the left side of (8) determined experimentally, which corresponded to the value of the final expression on the right side of (8) with a precision of approximately 1%.

The nucleation frequency was determined according to [17]:

$$I = \frac{DN_V}{a_0^2} \exp\left(\frac{-\Delta G^*}{kT}\right) \quad (9)$$

where D is the diffusion coefficient, $N_V = \rho N_A / \bar{M}$ is the average atomic concentration, \bar{M} is the average molar mass, and a_0 is the average interatomic spacing. The diffusion

coefficient was estimated using the technique from [42]; it turned out to be $3.6 \cdot 10^{-20} \text{ m}^2/\text{s}$. The average atomic concentration N_V was $8.66 \cdot 10^{28} \text{ m}^{-3}$. The average interatomic spacing was estimated from the Ehrenfest equation for a radius of the first coordination sphere, $a_0 = 2.5 \text{ \AA}$. The values necessary for further calculations are summarized in Table 1.

Table 1. Data used for the calculations.

Parameter	Value
$\frac{X_{\text{wire}}}{X_{\text{ribbon}}}$	1.2
u_c^{ribbon}	$2.23 \cdot 10^{-11} \text{ m/s}$
ΔG_{ch}	0.14 GJ/m^3
$E_\varepsilon(\sigma = 0)$	15.3 MJ/m^3
D	$3.6 \cdot 10^{-20} \text{ m}^2/\text{s}$
N_V	$8.66 \cdot 10^{28} \text{ m}^{-3}$
a_0	2.5 \AA

Taking into account Equations (5) and (9) can be rewritten as:

$$I = \frac{DN_V}{a_0^2} \exp\left(\frac{-16\pi\sigma^3}{3kT[\Delta G_{ch} + E_\varepsilon]^2}\right) \quad (10)$$

Calculations using (10) showed that the nucleation frequency of the ribbon was $1.9 \cdot 10^{17} \text{ m}^{-3}\text{s}^{-1}$, with a surface energy of 0.072 J/m^2 . The value of surface energy estimated in [18] for a Fe crystal in the amorphous environment at room temperature was 0.13 J/m^2 . This difference may be related to the purely homogeneous mechanism of crystal nucleation assumed in this work. However, nanocrystals are formed in this alloy not only by a homogeneous mechanism, but also by nucleation on Cu clusters. The estimated values of nucleation frequencies were quite close in the order of magnitude to $(10 \pm 5) \cdot 10^{19} \text{ m}^{-3}\text{s}^{-1}$ obtained under heat treatment at 763 K [24]. The distribution of nucleation frequencies over the microwire radius calculated from (12) is demonstrated in Figure 5.

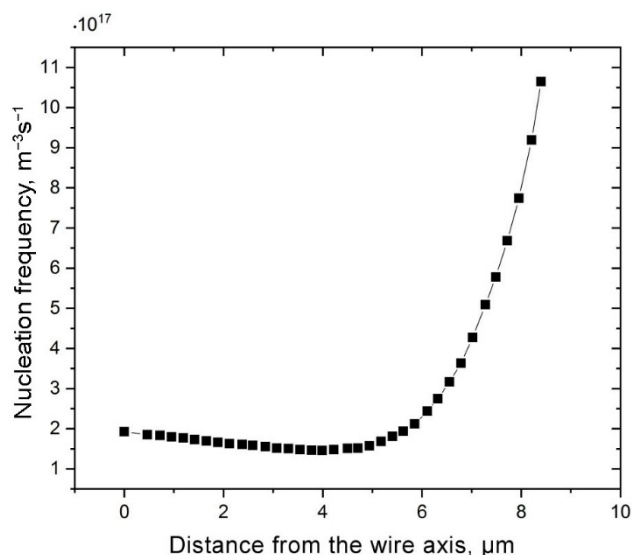


Figure 5. Distribution of nucleation frequency over the microwire radius.

The obtained distributions of the nucleation frequency and growth rate of the nanocrystals allowed for calculating the distribution of the crystallized volume fraction X over the microwire radius (Figure 6). One can see from Figure 6 that the volume fraction of the formed nanocrystals significantly increased in the near-surface region, where the value of compressive stresses can reach 2 GPa [6,8]. At that region, the average volume fraction

of nanocrystals in the microwire, calculated from the distribution in Figure 6, was about 29%. For the ribbon, the content of nanocrystals, calculated using the expression for the crystallized volume fraction X , was 24%, which was about 20% lower and corresponded to the experimentally revealed differences.

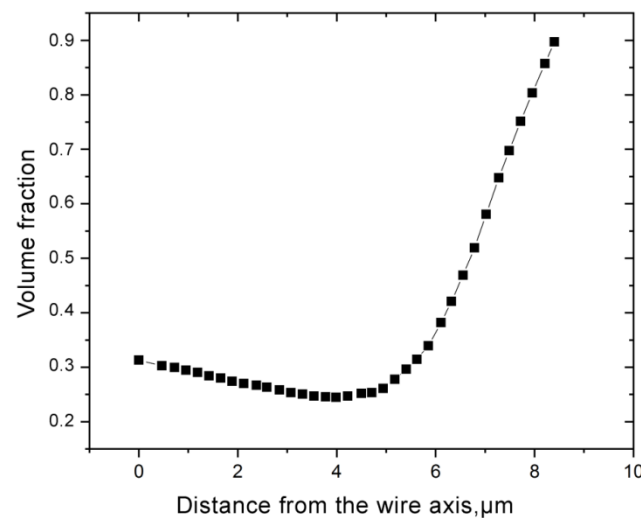


Figure 6. Volume fraction of the nanocrystalline phase depending on the microwire axis.

As one can see from Figure 2, at the initial crystallization stages, microwires crystallized more rapidly than ribbons. The obtained estimates suggested that, at early stages, nanocrystallization in microwires occurred predominantly in the microwire part where compressive inner stresses prevailed, i.e., in a small, near-surface region, which was about 2–2.5 μm for the microwire with a diameter of 16.8 μm . In addition, one of the reasons for the predominant crystallization of the surface layer could be not only compressive stresses, but also defects on the microwire surface.

In some amorphous alloys, compressive stresses can lead to different effects [43–46]. Due to compressive stresses, the slowdown of the crystallization kinetics led to an increase in the crystallization temperature in Pd-, La-, and Pr-based amorphous alloys. In such alloys, the glass transition temperature is below the crystallization temperature, $T_g < T_x$. This means that the crystallization of such alloys occurs from the supercooled liquid state, not from the amorphous state. During the nucleation and growth of crystals from the supercooled liquid state, the bulk effect may not affect the overall crystallization kinetics, due to the low viscosity of the alloy and rapid relaxation. In this case, a decrease in the diffusion coefficient (atomic mobility) may have played a decisive role. We assumed that the bulk effect played a crucial role in our case, since in the $\text{Fe}_{73.8}\text{Si}_{13}\text{B}_{9.1}\text{Cu}_1\text{Nb}_{3.1}$ alloy $T_g > T_x$ and crystallization occurs from the amorphous state, not from the supercooled liquid state. In this case, the viscosity of the alloy remains high and the stresses do not have time to relax. In addition, it should be noted that the effect of pressure on the crystallization of alloys with $T_g < T_x$ is not unambiguous. Thus, it was demonstrated in [17] that the application of bending stresses of more than 1.5 GPa to a $\text{Pd}_{40}\text{Cu}_{30}\text{Ni}_{10}\text{P}_{20}$ ribbon led to the fact that the tension side (above the neutral axis) of the glassy $\text{Pd}_{40}\text{Cu}_{30}\text{Ni}_{10}\text{P}_{20}$ ribbon showed no crystallinity. At the same time, the compressed part of the ribbon thickness showed the presence of nanocrystals. The bulk effect in Pd-based alloys is about 3 times lower than that in the $\text{Fe}_{73.8}\text{Si}_{13}\text{B}_{9.1}\text{Cu}_1\text{Nb}_{3.1}$ alloy. Therefore, we supposed that, in our case, the influence of the bulk effect on the crystallization was stronger.

The crystallization of the $\text{Fe}_{73.5}\text{Si}_{13.5}\text{B}_9\text{Cu}_1\text{Nb}_3$ alloy led to a simultaneous increase in the magnetic permeability and a decrease in the saturation magnetostriction [2,3]. Since the surface part of the microwire crystallized faster than its central part, the high-frequency properties of the microwire were improved in the surface part. For instance, there is the GMI effect, which is essentially an increase in the impedance Z of a soft magnetic

conductor placed in a static magnetic field. The GMI ratio $\Delta Z/Z$ of annealed amorphous-nanocrystalline $\text{Fe}_{73.5}\text{Si}_{13.5}\text{B}_9\text{Cu}_1\text{Nb}_3$ [47] and $\text{Fe}_{73.8}\text{Si}_{13}\text{B}_{9.1}\text{Cu}_1\text{Nb}_{3.1}$ [48] microwires increased significantly (up to 200%) in a wide range of frequencies, in comparison with as-prepared samples. It is noteworthy that the $\Delta Z/Z$ value depended on the depth of skin layer; the alternating current flows effectively in the near-surface region. The selection of heat treatment conditions could avoid the crystallization of the central part of the microwire during the crystallization of its surface part. In this case, the microwire would be a semblance of layered composite, with enhanced soft magnetic properties (like magnetic permeability) near the surface. This opens up new prospects for varying the high-frequency properties of $\text{Fe}_{73.5}\text{Si}_{13.5}\text{B}_9\text{Cu}_1\text{Nb}_3$ microwires and their application in modern sensorics.

5. Conclusions

It has been determined experimentally that the sizes and volume fraction of nanocrystals formed as a result of heat treatment at 753 K in the $\text{Fe}_{73.8}\text{Si}_{13}\text{B}_{9.1}\text{Cu}_1\text{Nb}_{3.1}$ microwires were greater than those in a ribbon. It was found that crystallization proceeded more intensively in the near-surface region of the microwire. These data are the evidence of different rates of crystallization processes in a microwire and a ribbon, which were caused by the presence of a high level of internal stresses in microwires.

The estimated calculations of the dependence of the nucleation frequency of Fe(Si) nanocrystals on mechanical stresses were carried out. Based on the performed calculations and the experimental data, it was found that the nucleation frequency of the nanocrystals in the near-surface region of a microwire increases significantly and reaches a maximum on the surface. The average value of nucleation frequency in an amorphous microwire was 1.5 times larger than that in a ribbon and was $2.9 \cdot 10^{17} \text{ m}^{-3}\text{s}^{-1}$.

The possibility of the formation of microwires during heat treatment with a predominant nucleation of nanocrystals in the near-surface region opens up broad prospects for controlling the high-frequency properties of microwires, and for using them as sensitive elements of strain and magnetic field sensors.

Author Contributions: Investigation, A.F. and O.A.; Supervision, A.A., G.A. and M.C.; Writing—original draft preparation, A.F.; Writing—review and editing, A.F., O.A., G.A. and A.A. All authors have read and agreed to the published version of the manuscript.

Funding: This work was supported by the Russian Science Foundation (grant no. 22-72-00067).

Informed Consent Statement: Not applicable.

Data Availability Statement: Not applicable.

Conflicts of Interest: The authors declare no conflict of interest.

References

1. Yoshizawa, Y.; Oguma, S.; Yamauchi, K. New Fe-based soft magnetic alloys composed of ultrafine grain structure. *J. Appl. Phys.* **1988**, *64*, 6044–6066. [[CrossRef](#)]
2. Chiriac, H.; Lupu, N.; Stoian, G.; Ababei, G.; Corodeanu, S.; Óvári, T.-A. Ultrathin Nanocrystalline Magnetic Wires. *Crystals* **2017**, *7*, 48. [[CrossRef](#)]
3. Herzer, G. Nanocrystalline soft magnetic materials. *Phys. Scr.* **1993**, *1993*, T49A. [[CrossRef](#)]
4. Carara, M.; Baibich, M.N.; Sommer, R.L. Stress level in Finemet materials studied by impedanciometry. *J. Appl. Phys.* **2002**, *91*, 8441–8443. [[CrossRef](#)]
5. Zhukov, A.; Ipatov, M.; Talaat, A.; Blanco, J.M.; Hernando, B.; Gonzalez-Legarreta, L.; Suñol, J.J.; Zhukova, V. Correlation of Crystalline Structure with Magnetic and Transport Properties of Glass-Coated Microwires. *Crystals* **2017**, *7*, 41. [[CrossRef](#)]
6. Chiriac, H.; Ovari, T.A.; Pop, G. Internal stress distribution in glass-covered amorphous magnetic wires. *Phys. Rev. B* **1995**, *52*, 10104–10113. [[CrossRef](#)]
7. Baranov, S.A.; Larin, V.S.; Torcunov, A.V. Technology, Preparation and Properties of the Cast Glass-Coated Magnetic Microwires. *Crystals* **2017**, *7*, 136. [[CrossRef](#)]
8. Aksenov, O.I.; Fuks, A.A.; Aronin, A.S. The effect of stress distribution in the bulk of a microwire on the magnetization processes. *J. Alloys Compd.* **2020**, *836*, 155472. [[CrossRef](#)]

9. Morchenko, A.T.; Panina, L.V.; Larin, V.S.; Churyukanova, M.N.; Salem, M.M.; Hashim, H.; Trukhanov, A.V.; Korovushkin, V.V.; Kostishyn, V.G. Structural and magnetic transformations in amorphous ferromagnetic microwires during thermomagnetic treatment under conditions of directional crystallization. *J. Alloys Compd.* **2017**, *698*, 685–691. [CrossRef]
10. Evstigneeva, S.; Morchenko, A.; Trukhanov, A.; Panina, L.; Larin, V.; Volodina, N.; Yudanov, N.; Nematov, M.; Hashim, H.; Ahmad, H. Structural and magnetic anisotropy of directionally-crystallized ferromagnetic microwires. *EPJ Web Conf.* **2018**, *185*, 04022. [CrossRef]
11. Panina, L.; Dzhumazoda, A.; Nematov, M.; Alam, J.; Trukhanov, A.; Yudanov, N.; Morchenko, A.; Rodionova, V.; Zhukov, A. Soft Magnetic Amorphous Microwires for Stress and Temperature Sensory Applications. *Sensors* **2019**, *19*, 5089. [CrossRef] [PubMed]
12. Li, Z.-D.; Zhang, W.-W.; Li, G.-T.; Li, S.-S.; Ding, H.-S.; Zhang, T.; Song, Y.-J. Magnetic field annealing of FeCo-based amorphous alloys to enhance thermal stability and Curie temperature. *Rare Met.* **2018**, 1–7. [CrossRef]
13. Serrano, I.G.; Hernando, A.; Marín, P. Low temperature magnetic behavior of glass-covered magnetic microwires with gradient nanocrystalline microstructure. *J. Appl. Phys.* **2014**, *115*, 033903. [CrossRef]
14. Parsons, R.; Ono, K.; Li, Z.; Kishimoto, H.; Shoji, T.; Kato, A.; Hill, M.R.; Suzuki, K. Prediction of density in amorphous and nanocrystalline soft magnetic alloys: A data mining approach. *J. Alloys Compd.* **2021**, *859*, 157845. [CrossRef]
15. The Materials Project. Available online: <https://materialsproject.org/materials/mp-2199/> (accessed on 19 September 2022).
16. Yan, Z.; Song, K.; Hu, Y.; Dai, F.; Chu, Z.; Eckert, J. Localized crystallization in shear bands of a metallic glass. *Sci. Rep.* **2016**, *6*, 19358. [CrossRef] [PubMed]
17. Yavari, A.R.; Georganakis, K.; Antonowicz, J.; Stoica, M.; Nishiyama, N.; Vaughan, G.; Chen, M.; Pons, M. Crystallization during bending of a Pd-based metallic glass detected by X-ray microscopy. *Phys. Rev. Lett.* **2012**, *109*, 085501. [CrossRef] [PubMed]
18. Gheiratmand, T.; Hosseini, H.R.M.; Davami, P.; Ababei, G.; Song, M. Mechanism of mechanically induced nanocrystallization of amorphous FINEMET ribbons during milling. *Met. Mater. Trans. A* **2015**, *46*, 2718–2725. [CrossRef]
19. Aronin, A.S.; Abrosimova, G.E. Reverse martensite transformation in iron nanocrystals under severe plastic deformation. *Mater. Lett.* **2012**, *83*, 183–185. [CrossRef]
20. Vasil'ev, L.S.; Lomaev, I.L. On possible mechanisms of nanostructure evolution upon severe plastic deformation of metals and alloys. *Phys. Met. Metallogr.* **2006**, *101*, 386–392. [CrossRef]
21. Ye, F.; Lu, K. Pressure effect on crystallization kinetics of an Al–La–Ni amorphous alloy. *Acta Mater.* **1999**, *47*, 2449–2454. [CrossRef]
22. Lee, S.-W.; Huh, M.-Y.; Fleury, E.; Lee, J.-C. Crystallization-induced plasticity of Cu–Zr containing bulk amorphous alloys. *Acta Mater.* **2006**, *54*, 349–355. [CrossRef]
23. Noh, T.H.; Lee, M.B.; Kim, H.J.; Kang, I.K. Relationship between crystallization process and magnetic properties of Fe-(Cu-Nb)-Si-B amorphous alloys. *J. Appl. Phys.* **1990**, *67*, 5568–5570. [CrossRef]
24. Clavaguera, N.; Pradell, T.; Jie, Z.; Clavaguera-Mora, M.T. Thermodynamic and kinetic factors controlling the formation of nanocrystalline FeCuNbSiB materials. *Nanostruct. Mater.* **1995**, *6*, 453–456. [CrossRef]
25. Luborsky, F.; Walter, J. Stress relaxation in amorphous alloys. *Mater. Sci. Eng.* **1978**, *35*, 255–261. [CrossRef]
26. Guinier, A. *Theorie et Technique de la Radiocristallographie*; Dumond: Paris, France, 1956.
27. Cruz, M.E.; Li, J.; Gorni, G.; Durán, A.; Mather, G.C.; Balda, R.; Fernández, J.; Castro, Y. Crystallization Process and Site-Selective Excitation of Nd³⁺ in LaF₃/NaLaF₄ Sol–Gel-Synthesized Transparent Glass-Ceramics. *Crystals* **2021**, *11*, 464. [CrossRef]
28. Abrosimova, G.E.; Aronin, A.S.; Kholstinina, N.N. On the determination of volume fraction of the crystalline phase in amorphous-crystalline alloys. *Phys. Solid State* **2010**, *52*, 445–451. [CrossRef]
29. Vásquez, M.; Marín, P.; Davies, H.A.; Olofinjana, A. Magnetic hardening of FeSiBCuNb ribbons and wires during the first stage of crystallization to a nanophase structure. *Appl. Phys. Lett.* **1994**, *64*, 3184–3186. [CrossRef]
30. Cahn, R.W.; Haasen, P. *Physical Metallurgy*, 3rd ed.; North-Holland Physics Publishing: Amsterdam, The Netherlands, 1983.
31. Duong, A.H.; Malkinski, L.; Grossinger, R. Magnetomechanical properties in FINEMET type alloy. In Proceedings of the VACETS Technical International Conference, San Jose, CA, USA, 17–19 July 1997; p. 40.
32. Kikuchi, M.; Fukamichi, K.; Masumoto, T. Young's modulus and delay time characteristics of ferromagnetic Fe-Si-B amorphous alloys. *Sci. Rep. Res. Inst. Tohoku Univ.* **1976**, *26*, 232–239.
33. Yang, G.N.; Sun, B.A.; Chen, S.Q.; Gu, J.L.; Shao, Y.; Wang, H.; Yao, K.F. Understanding the effects of Poisson's ratio on the shear band behavior and plasticity of metallic glasses. *J. Mater. Sci.* **2017**, *52*, 6789–6799. [CrossRef]
34. Bansal, N.P.; Doremus, R.H. *Handbook of Glass Properties*; Academic Press: Cambridge, MA, USA, 1986.
35. Gheiratmand, T.; Hosseini, H.R.M. Finemet nanocrystalline soft magnetic alloy: Investigation of glass forming ability, crystallization mechanism, production techniques, magnetic softness and the effect of replacing the main constituents by other elements. *J. Magn. Magn. Mater.* **2016**, *408*, 177–192. [CrossRef]
36. Thompson, C.; Spaepen, F. On the approximation of the free energy change on crystallization. *Acta Metall.* **1979**, *27*, 1855–1859. [CrossRef]
37. Antoszewska, M.; Wasiak, M.; Gwizdała, T.; Sovak, P.; Moneta, M. Thermal induced structural and magnetic transformations in Fe_{73.5-x}Ce_{x=0,3,5,7}Si_{13.5}B₉Nb₃Cu₁ amorphous alloy. *J. Therm. Anal. Calorim.* **2014**, *115*, 1381–1386. [CrossRef]
38. Clavaguera-Mora, M.T.; Clavaguera, N.; Crespo, D.; Pradell, T. Crystallisation kinetics and microstructure development in metallic systems. *Prog. Mater. Sci.* **2002**, *47*, 559–619. [CrossRef]
39. Nishiyama, N.; Inoue, A. Supercooling investigation and critical cooling rate for glass formation in Pd–Cu–Ni–P alloy. *Acta Mater.* **1999**, *47*, 1487–1495. [CrossRef]

40. Uhlmann, D.R. A kinetic treatment of glass formation. *J. Non Cryst. Solids* **1972**, *7*, 337–348. [[CrossRef](#)]
41. Christian, J.W. *The Theory of Phase Transformations in Metals and Alloys*; Pergamon Press: Oxford, UK, 1965.
42. Pershina, E.; Matveev, D.; Abrosimova, G.; Aronin, A. Formation of nanocrystals in an amorphous Al₉₀Y₁₀ alloy. *Mat. Char.* **2017**, *133*, 87–93. [[CrossRef](#)]
43. Jiang, J.Z.; Zhuang, Y.X.; Rasmussen, H.; Nishiyama, N.; Inoue, A.; Lathe, C. Crystallization of Pd₄₀Cu₃₀Ni₁₀P₂₀ bulk glass under pressure. *Eur. Lett.* **2001**, *54*, 182. [[CrossRef](#)]
44. Jiang, J.Z.; Saksl, K.; Nishiyama, N.; Inoue, A. Crystallization in Pd₄₀Ni₄₀P₂₀ glass. *J. Appl. Phys.* **2002**, *92*, 3651–3656. [[CrossRef](#)]
45. Wang, Y.; Zhao, W.; Li, G.; Li, Y.; Liu, R. Structural evolution of Lanthanide-based metallic glasses under high-pressure annealing. *J. Alloys Compd.* **2013**, *551*, 185–188. [[CrossRef](#)]
46. Falqui, A.; Loche, D.; Casu, A. In Situ TEM Crystallization of Amorphous Iron Particles. *Crystals* **2020**, *10*, 41. [[CrossRef](#)]
47. Knobel, M.; Sánchez, M.L.; Gómez-Polo, C.; Marin, P.; Vazquez, M.; Hernando, A. Giant magneto-impedance effect in nanostructured magnetic wires. *J. Appl. Phys.* **1996**, *79*, 1646–1654. [[CrossRef](#)]
48. Talaat, A.; Zhukova, V.; Ipatov, M.; Blanco, J.M.; Gonzalez-Legarreta, L.; Hernando, B.; del Val, J.J.; González, J.; Zhukov, A. Optimization of the giant magnetoimpedance effect of Finemet-type microwires through the nanocrystallization. *J. Appl. Phys.* **2014**, *115*, 17A313. [[CrossRef](#)]